

Rift topography linked to magmatism at the intermediate spreading Juan de Fuca Ridge

Suzanne M. Carbotte Lamont-Doherty Earth Observatory, Palisades, New York 10964, USA
Robert S. Detrick Woods Hole Oceanographic Institution, Woods Hole, Massachusetts 02543, USA
Alistair Harding Scripps Institution of Oceanography, La Jolla, California 92093, USA
Juan Pablo Canales Woods Hole Oceanographic Institution, Woods Hole, Massachusetts 02543, USA
Jeffrey Babcock } Scripps Institution of Oceanography, La Jolla, California 92093, USA
Graham Kent }
Emily Van Ark Woods Hole Oceanographic Institution, Woods Hole, Massachusetts 02543, USA
Mladen Nedimovic } Lamont-Doherty Earth Observatory, Palisades, New York 10964, USA
John Diebold }

ABSTRACT

New seismic observations of crustal structure along the Juan de Fuca Ridge indicate that the axial rift topography reflects magma-induced deformation rather than alternating phases of magmatism and tectonic extension, as previously proposed. Contrary to predictions of the episodic models, crustal magma bodies are imaged beneath portions of all ridge segments surveyed at average depths of 2.1–2.6 km. The shallow rift valley or axial graben associated with each Juan de Fuca segment is ~50–200 m deep and 1–8 km wide and is well correlated with a magma body in the subsurface. Analysis of graben dimensions (height and width) shows that the axial graben narrows and graben height diminishes where the magma body disappears, rather than deepening and broadening, as expected for rift topography due to tectonic extension. We propose an evolutionary model of axial topography that emphasizes the contribution of dike intrusion to subsidence and fault slip at the seafloor. In this model an evolving axial topography results from feedbacks between the rheology of the crust above a magma sill and dike intrusion, rather than episodic magma delivery from the mantle.

Keywords: Juan de Fuca Ridge, magma chambers, dikes, faulting, spreading centers.

INTRODUCTION

The formation of oceanic crust at mid-ocean ridges involves the production of melts in the upper mantle through what is probably a continuous process of adiabatic melting and porous flow. Once melt reaches crustal levels, melt is extracted during discrete events; dike injection from mid-crustal melt bodies builds the sheeted dike section of the upper crust,

and possibly subcrustal melt sills build the layered gabbros of the lower crust (e.g., Kelemen et al., 1997). Melt transport and extraction from the mantle may be episodic; some studies of ridge axis structure and lava chemistry indicate crustal accretion during intermittent magmatic phases (e.g., Lewis, 1979; Tucholke and Lin, 1994). Kappel and Ryan (1986) attributed the marked variations in

ridge morphology along the Juan de Fuca Ridge to non-steady-state accretion through alternating magmatic-tectonic phases. Since then, the Juan de Fuca Ridge has been widely cited as a type example for episodic magmatism in ongoing debate over the steady-state versus non-steady-state nature of crustal formation (e.g., Pezard et al., 1992; Wilcock and Delaney, 1996; Perfit and Chadwick, 1998).

The Juan de Fuca Ridge comprises seven segments, each with a distinct axial morphology (Fig. 1). Cleft, the southernmost segment, has a shallow and broad axial high notched by a 2–3-km-wide axial rift flooded with recent lavas. Within Vance, the next segment to the north, an axial volcanic ridge (AVR) is located in the center of a much broader, ~8 km wide, valley. A narrow 1–2-km-wide depression bisects the crest of a narrow and deeper axial high at the Northern Symmetric (or Cobb) segment. At Endeavour segment, abundant faulting is observed in the floor of a 2–3-km-wide axial trough; there is little evidence for recent eruptions. In the Kappel and Ryan (1986) model, these ridge segments are each in a different phase in a cycle of alternating magmatism and tectonism. An AVR is formed

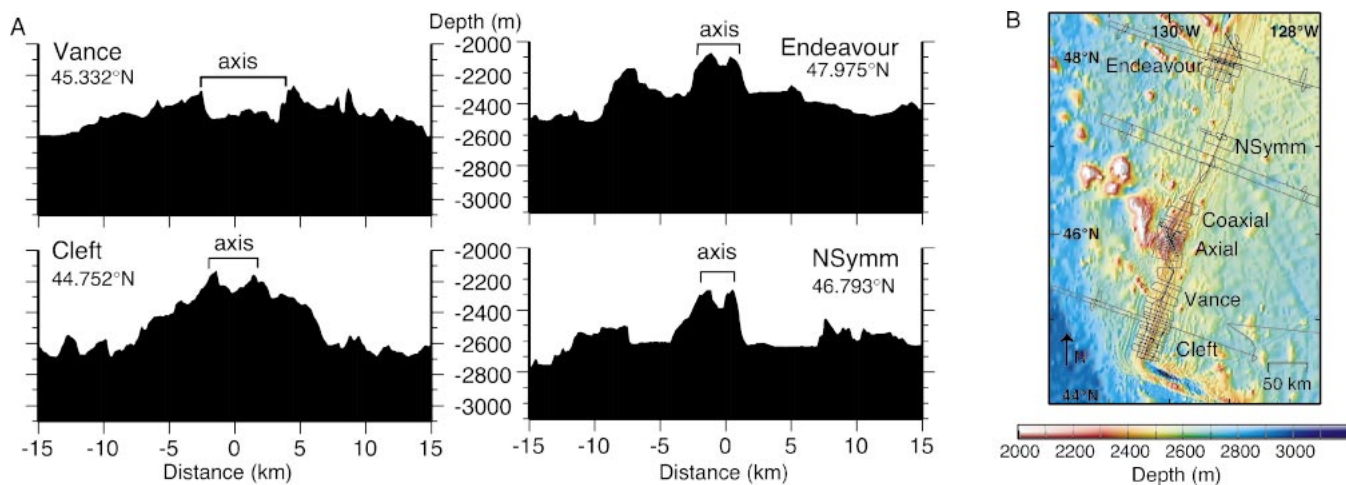


Figure 1. A: Cross-axis bathymetry profiles showing contrast in ridge morphology at adjacent ridge segments. Latitude of profile crossing at axis is indicated. B: Regional bathymetry for Juan de Fuca Ridge; track of seismic survey is overlain.

at the axis during a magmatic phase (Vance), and is split tectonically as magmatism wanes to form a shallow axial depression (Cleft). With ongoing tectonism and intermittent magmatism, this depression widens (Northern Symmetric and Endeavour) until a new magmatic phase initiates construction of a new AVR. The abyssal hills on the flanks of the Juan de Fuca Ridge were interpreted by Kappel and Ryan (1986) as split AVRs formed at the axis during these major magmatic phases.

In this study we present new observations on the crustal structure of the Juan de Fuca Ridge from the first detailed seismic reflection study carried out in the region (Fig. 1). Data were collected along the entire length of the ridge axis south from Endeavour segment, with detailed surveys of Endeavour, Vance, Cleft, and Axial Volcano, and along three long ridge flank transects. Our observations of seismic layer 2A and the presence and depth of magma bodies provide insights into the magmatic state of each Juan de Fuca Ridge segment and allow us to test the alternating magmatic-tectonic cycle model for ridge structure. Here we focus on segment to segment differences in axial structure. Details on ridge-axis structure within Cleft and Vance segments and description of the seismic experiment are in Canales et al. (2005; see also the GSA Data Repository¹).

RESULTS FROM SEISMIC OBSERVATIONS

Seismic reflection profiles reveal a strong reflection, believed to correspond with a magma sill associated with the axial magma chamber (AMC; Detrick et al., 1987), beneath all Juan de Fuca Ridge segments including Northern Symmetric (NSymm), where the axial high is narrowest and in places difficult to identify (Figs. 1 and 2). With the exception of Axial Volcano (0.6–1.2 s two-way traveltime [twtt]; Kent et al., 2003), the AMC at this intermediate spreading ridge is deeper within the crust (~0.8–1.0 s twtt or ~2–2.5 km) than at the fast spreading East Pacific Rise (EPR), consistent with predictions of theoretical models of crustal accretion (Phipps Morgan and Chen, 1993). The depth of the AMC reflection varies from segment to segment; the shallowest (excluding Axial Volcano) and most uniform depths are beneath Cleft segment (average 2055 m, standard deviation ± 70 m), and the deepest and most variable is beneath Endeavour segment (2584 ± 330 m, Fig. 2D). Average magma sill depth beneath NSymm

and Vance segments, which represent extremes in ridge axis morphology along the Juan de Fuca Ridge, differ by <50 m. Excluding the overlapped portions of segments, the magma body is detected beneath 60% of the ridge axis, remarkably similar to findings at the EPR (Detrick et al., 1987).

The base of seismic layer 2A, often interpreted as the boundary between the extrusive and dike sections (e.g., Karson and Christeson, 2002), is well imaged throughout the region. There are segment-to-segment differences in the average thickness of layer 2A along the axis (Fig. 2E); the thinnest and most uniform is at Cleft segment (219, ± 40 m), and a thicker and more variable 2A is beneath the Endeavour segment (322, ± 90 m). Uncertainties in depth estimates are ± 50 m for layer 2A and ± 70 m for the AMC (Canales et al., 2005).

The shallow rift valley or axial graben found at each Juan de Fuca Ridge segment is defined by remarkably linear parallel walls that extend for part or all of each segment. Here we prefer the term axial graben to distinguish this feature from the much larger relief (500 m to several kilometers) rift valleys found at slow spreading ridges. Axial graben dimensions (height and width) are measured for comparison with observations on internal crustal structure (Figs. 2B, 2C). Graben width differs between segments with abrupt steps of several kilometers marking segment boundaries. Smaller steps in graben width (<1 km) are found within segments, separating sections of approximately uniform or continuously varying width that extend for tens of kilometers. At the two segments with the widest grabens (>6 km), Vance and Coaxial, low-relief (as much as ~100 m) AVRs mark the zone of active volcanism.

Graben height varies within each segment and ranges from <50 m to ~250 m. In all cases, the axial graben diminishes in relief near segment ends (Fig. 2B) or becomes asymmetric with one wall disappearing. At several segments, systematic along-axis variations in graben height form humped graben height profiles (Fig. 2B). Graben height minimums separating adjacent humped sections typically coincide with changes in graben width and may define a third-order segmentation of the Juan de Fuca Ridge in the classification scheme of Macdonald et al. (1988).

Within each Juan de Fuca Ridge segment, a close spatial association is found between where an axial magma body is imaged and where the axial graben is well defined. With the exception of south Vance, a magma sill is consistently present where graben height is greatest along a segment (Figs. 2A, 2B), whereas the graben diminishes in relief where the magma body disappears toward segment

ends. A prominent example of this relationship is found at the Split or Surveyor seamount, a rifted conical seamount as high as 475 m, ~7 km in diameter, and centered on the axis at the north end of NSymm segment (Fig. 2; Fig. DR1 [see footnote 1]). No magma body is detected for ~25 km south of Split seamount where the axis is subducted and a linear axial graben >25 m in relief is not present. However, directly beneath Split Seamount, where steep fault scarps bound a 3–5-km-wide, 250-m-deep graben, there is a strong isolated AMC reflection. Similarly, at Endeavour segment, a magma body is only detected under the central shallow portion of the ridge segment where the axial graben is well defined by two parallel axis-facing scarps. In some cases, the fine-scale segmentation of the axial graben defined by along-axis changes in graben dimensions coincides with segmentation of the AMC (Fig. 2). For example, a break in the AMC reflection suggests that separate magma sills underlie north and south Cleft (Canales et al., 2005). This discontinuity in the AMC coincides with segmentation of the axial graben defined by the graben height profile, suggesting differences in the history of graben growth associated with each magma sill.

DISCUSSION

Contrary to predictions of the magmatic-tectonic model of Kappel and Ryan (1986), seismic observations reveal that magma bodies are present beneath portions of each Juan de Fuca Ridge segment, including those previously assumed to be in a tectonic phase. Each segment is associated with a distinct magmatic system with a magma body at different depths in the crust. The zero-age thickness of the seismically inferred extrusive layer (layer 2A) also varies from segment to segment; thicker 2A is present where the magma sill is deeper (Figs. 2D–2E), consistent with the model of Buck et al. (1997) and suggesting magmatic controls on extrusive layer thickness.

Our observations indicate that the axial rift relief along the Juan de Fuca Ridge is also linked to magmatic processes, with a close correlation between the location of the axial graben and a crustal magma sill and coincident fine-scale segmentation of both features. If the axial rift were a tectonically generated feature, as is commonly assumed, it is expected to be well developed in regions where the magma body is absent, and where continuous plate separation should be accommodated by tectonic extension. Instead, the opposite relationship is observed. Where the magma body is absent, the symmetric axial graben disappears. Furthermore, for rift topography generated by tectonic stretching, wider and deeper grabens are predicted where the brittle

¹GSA Data Repository item 2006039, description of seismic experiment and map view showing extent of magma lens beneath Endeavour segment and Split Seamount, is available online at www.geosociety.org/pubs/ft2006.htm, or on request from editing@geosociety.org or Documents Secretary, GSA, P.O. Box 9140, Boulder, CO 80301, USA.

Figure 2. A: Along-axis profile showing two-way traveltime (twtt) to sea-floor (black), base of layer 2A (blue), and axial magma chamber (AMC, red). Vertical lines show primary segment boundaries (bold lines) and possible third-order segments (short light lines). B: Along-axis height of axial graben (black dots). Graben dimensions are measured from bathymetric profiles projected perpendicular to ridge axis and spaced 300 m apart. We identify axial graben where two linear axis-facing scarps >25 m high bound axis. Except for segments with axial volcanic ridge (AVR), graben height is measured as difference between seafloor depth at axis and at top of graben walls, averaged for both walls. Where AVR is present within Coaxial and Vance segments, we add height of AVR above graben floor. Red line shows AMC depth below seafloor converted from twtt, assuming velocities of 2.26 for 2A and 5.5 km/s for seismic layer 2B. C: Graben width (black dots) measured as distance between tops of graben walls. Red line shows $2 \times$ AMC depth for comparison with graben width (see text). D: Average AMC depth and (E) on-axis 2A thickness with standard deviation (bars) and minimum and maximum range (open circles) for each ridge segment. Averages are plotted at latitude of segment midpoints.

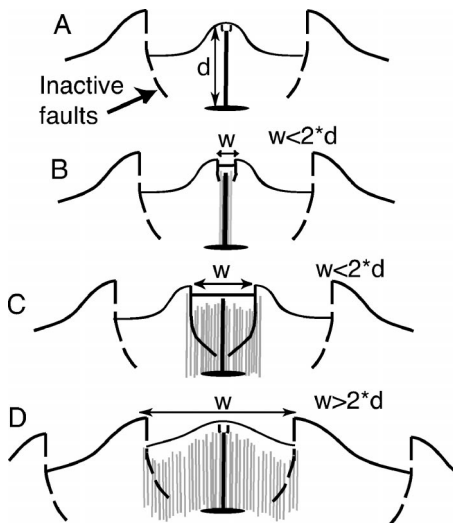
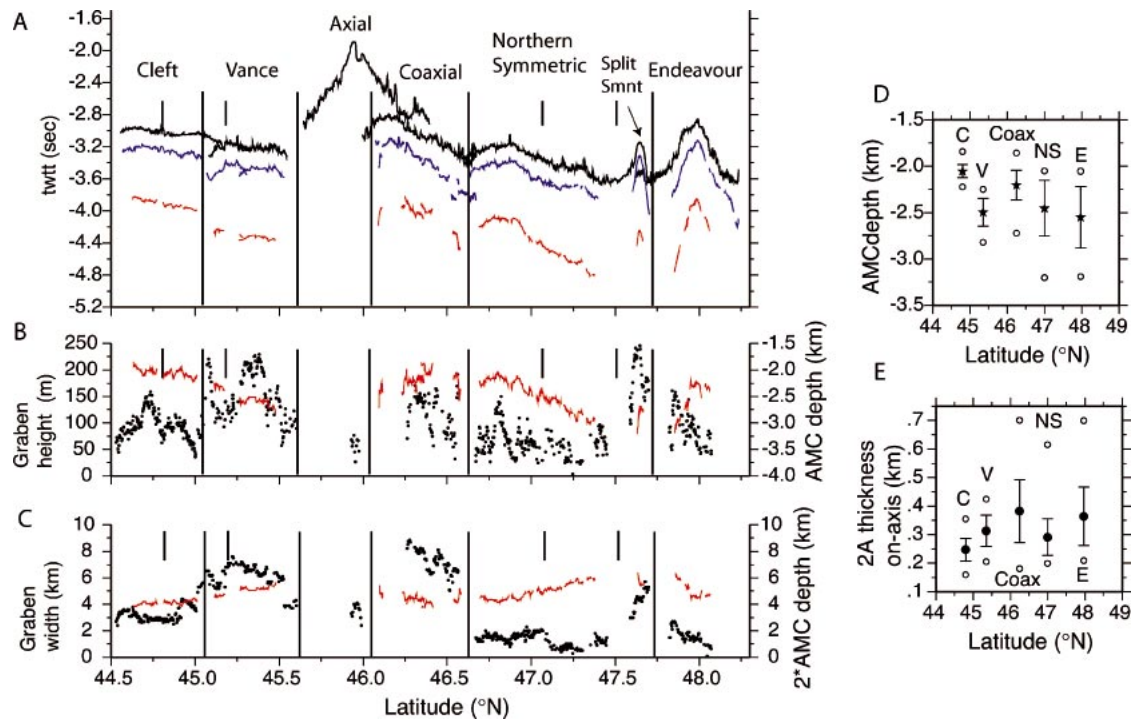


Figure 3. Evolutionary model for axial rift topography (see text). A: Narrow grabens form above dikes during dike intrusion and are readily buried by lavas contributing to axial volcanic ridge (AVR) relief. B, C: With ongoing dike intrusion, fault slip becomes localized on preferred graben faults, which grow with successive dike events. Graben widens and eruptions become confined by graben walls. D: Graben faults cease to be active as they are transported beyond zone of influence of stress perturbations due to dikes intruded from magma sill. New AVR construction begins.

layer is thicker (e.g., Shaw and Lin, 1996). However, at the Juan de Fuca Ridge, graben width differs markedly from segment to segment where the brittle layer thickness inferred from magma sill depths is similar (e.g., Vance, NSymm, Fig. 2), and maximum graben heights are typically found where the brittle layer is thinnest, not thickest. The axial graben does not deepen and widen toward segment ends, as is typical of rift valleys on the slow spreading Mid-Atlantic Ridge (e.g., Shaw and Lin, 1996), but rather diminishes in relief toward the ends of segments as the magma body disappears.

RIFT TOPOGRAPHY AND MAGMATIC PROCESSES

Where magma is present in the crust and the lithosphere is under continuous far-field extension, dike injection is expected to occur before compressive stresses within the brittle layer above a magma body are low enough to give rise to normal faulting (e.g., Rubín, 1992). With magma bodies in the crust at all Juan de Fuca Ridge segments, normal faulting within the axial zone due to tectonic extension may be rare. This notion is supported by the lack of seismicity observed along the axis of the Juan de Fuca Ridge during the past ~15 yr of hydroacoustic monitoring, except during dike injection events (Dziak et al., 1995; Bohnenstiehl et al., 2004).

Observations from subareal settings indi-

cate that dike intrusion can lead to surface faulting with subsidence of grabens up to several kilometers wide during single intrusion events (Rubín and Pollard, 1988; Rubín, 1992). Dike-induced faulting at oceanic spreading centers has been invoked to account for narrow (10–100 m) grabens formed during eruptions at Cleft and Coaxial segments (Chadwick and Embley, 1998). Models of the mechanical effects of dike emplacement predict dike-induced stresses in the surrounding crust with a zone of enhanced compression adjacent to the walls of a dike and tension above the dike top (Rubín and Pollard, 1988; Chadwick and Embley, 1998). Rubín (1992) proposed that enhanced tension can trigger fault slip and graben subsidence ahead of a propagating dike on deep preexisting fault planes as the zone of enhanced tension migrates during intrusion, as well as above the dike top. Based on observations at Krafla, Rubín (1992) attributed the tendency for dike-induced slip to occur on deep faults versus above a dike to local stress conditions related to the recent tectonic history.

Building on these observations, we suggest that dike-induced faulting may play a key role in the formation of the axial rift at the Juan de Fuca Ridge. In the first stage of our model (Fig. 3), narrow grabens form in the shallow crust above dikes during intrusion centered beneath an AVR. Eruptions readily flood these grabens, feeding lavas to the flanks of the

AVR and contributing to AVR relief and the observed off-axis thickening of layer 2A (Canales et al., 2005). With ongoing dike intrusion, surface deformation becomes localized on graben-bounding faults and fault planes deep as tensile stress perturbations associated with propagating dikes from the magma sill trigger repeated fault slip on these planes of weakness. The axial graben widens through ongoing intrusion, and volcanic eruptions become confined by the graben walls. Ambient stress conditions in the crust are expected to evolve as dike intrusion events induce local compression, which is relieved by ongoing far-field extension. As a result, favorable stress conditions for fault slip on deep faults bounding wide grabens may be present only intermittently and will depend on dike frequency.

Mechanical models predict that the width of the zone of enhanced tension ahead of a dike will vary as a function of dike dimensions and depth to the dike top with a maximum width of surface deformation of roughly twice dike depth (e.g., Rubin, 1992). From these models, we expect the width of dike-induced faulting at the surface to be limited by maximum dike depth, which is constrained by magma sill depth. The width of the axial graben at Cleft, Nsymm, and Endeavour segments is less than twice magma sill depth (Fig. 2C), and graben-bounding faults at these segments may continue to slip during magmatic events under favorable stress conditions.

Vance and Coaxial segments have axial grabens wider than twice the depth to the underlying magma body (Fig. 2C) and both are currently in an AVR building phase. Following thermal models of Phipps Morgan and Chen (1993), shallower magma bodies would be expected beneath these segments if AVRs are constructed during periods of enhanced magmatism, as proposed by Kappel and Ryan (1986), but this is not observed. In our model, AVR formation is initiated when ongoing dike emplacement has transported graben-bounding faults beyond the region of influence of dike-induced stress perturbations at depth (Fig. 3D). We speculate that voluminous eruptions may be favored, contributing to AVR formation, when slip on widely spaced graben faults ceases, and large tensile stress accumulations can occur with ongoing far-field extension. A crustal magma sill is assumed present at the axis at all stages of the model and at similar depths in the mid-crust. With ongoing crustal accretion, the split AVRs that form the shoulders of the axial graben are transported off axis to form the ridge flank abyssal hills.

CONCLUSIONS

Our model for axial topography along the Juan de Fuca Ridge involves an evolutionary

cycle from an AVR to a wide axial graben. In contrast to previous models that invoke episodic magma delivery from the mantle, we attribute this evolving topography to fault slip and surface deformation during dike intrusion from a steady-state crustal magma sill. Curewitz and Karson (1998) speculated that differences in the frequency of dike intrusion at fast and slow spreading ridges and resultant impact on stress conditions in the crust may contribute to the large-scale differences in axial structure observed. At fast spreading rates, frequent dike injection may keep ambient compressive stresses too high for significant fault slip to occur during dike events, leading to axial relief dominated by volcanic eruptions. At slow spreading ridges, magma bodies may reside only intermittently beneath segment centers, and much of the large-scale axial valley relief likely evolves through tectonic extension. Our results from the Juan de Fuca Ridge suggest that dike intrusion may be frequent enough here that favorable stress conditions for fault slip are achieved primarily during dike events, leading to a prominent axial graben formed by axial magmatism. The existence of stress conditions conducive to dike-induced faulting may be a defining characteristic of crustal accretion at intermediate spreading ridges.

ACKNOWLEDGMENTS

We thank Bill Ryan, Del Bohnenstiehl, and Ken Macdonald for fruitful discussions, and Mike Perfit, William Wilcock, and an anonymous reviewer for thoughtful reviews. This research was supported by National Science Foundation grants OCE-00-02488, OCE-00-02551, and OCE-00-02600. Lamont-Doherty Earth Observatory contribution 6840.

REFERENCES CITED

- Bohnenstiehl, D.R., Dziak, R., Tolstoy, M., Fox, C.G., and Fowler, M., 2004, Temporal and spatial history of the 1999–2000 Endeavour Segment seismic series, Juan de Fuca Ridge: G-cubed, v. 5, p. Q09003, doi: 10.1029/2004GC000735.
- Buck, R.W., Carbotte, S.M., and Mutter, C.Z., 1997, Controls on extrusion at mid-ocean ridges: *Geology*, v. 25, p. 935–938.
- Canales, J.P., Detrick, R.S., Carbotte, S.M., Kent, G.M., Diebold, J.B., Harding, A., Babcock, J., Nedimovic, M., and van Ark, E., 2005, Upper crustal structure and axial topography at intermediate-spreading ridges: Seismic constraints from the southern Juan de Fuca Ridge: *Journal of Geophysical Research*, vol. 110, doi: 10.1029/2005JB003630.
- Chadwick, W.W., and Embley, R.W., 1998, Graben formation associated with recent dike intrusions and volcanic eruptions on the mid-ocean ridge: *Journal of Geophysical Research*, v. 103, p. 9807–9825.
- Curewitz, D., and Karson, J.A., 1998, Geological consequences of dike intrusion at mid-ocean ridge spreading centers, in Buck, W.R., et al., eds., *Faulting and magmatism at mid-ocean ridges*: American Geophysical Union Geophysical Monograph 106, p. 117–136.
- Detrick, R.S., Buhl, P., Vera, E., Mutter, J., Orcutt, J., Madsen, J., and Brocher, T., 1987, Multichannel seismic imaging of a crustal magma chamber along the East Pacific Rise: *Nature*, v. 326, p. 35–41.

- Dziak, R.P., Fox, C.G., and Schreiner, A.E., 1995, The June–July 1993 seismo-acoustic event at CoAxial segment, Juan de Fuca Ridge: Evidence for a lateral dike injection: *Geophysical Research Letters*, v. 22, p. 135–138.
- Kappel, E.S., and Ryan, W.B.F., 1986, Volcanic episodicity and a non-steady state rift valley along the northeast Pacific spreading centers: Evidence from SeaMARC I: *Journal of Geophysical Research*, v. 91, p. 13,925–13,940.
- Karson, J.A., and Christeson, G., 2002, Comparison of geological and seismic structure of uppermost fast-spread oceanic crust: Insights from a crustal cross-section at the Hess Deep Rift, in Goff, J., and Holliger, K., eds., *Heterogeneity in the crust and upper mantle: Nature, scaling and seismic properties*: New York, Kluwer Academic, 358 p.
- Kelemen, P.B., Koga, K., and Shimizu, N., 1997, Geochemistry of gabbro sills in the crust-mantle transition zone of the Oman ophiolite: Implications for the origin of the oceanic lower crust: *Earth and Planetary Science Letters*, v. 146, p. 475–488.
- Kent, G., Harding, A., Babcock, J., Orcutt, J., Carbotte, S., Diebold, J., Nedimovic, M., Detrick, R., Canales, P., and Van Ark, E., 2003, A new view of 3-D magma chamber structure beneath axial seamount and coaxial segment: Preliminary results from the 2002 Multichannel Seismic Survey of the Juan de Fuca Ridge: *Eos (Transactions, American Geophysical Union)*, v. 84, p. B12A–0755.
- Lewis, B.T.R., 1979, Periodicities in volcanism and longitudinal magma flow on the East Pacific Rise at 23°N: *Geophysical Research Letters*, v. 10, p. 753–756.
- Macdonald, K.C., Fox, P.J., Perram, L.J., Eisen, M.F., Haymon, R.M., Miller, S.P., Carbotte, S.M., Cormier, M.-H., and Shor, A.N., 1988, A new view of the mid-ocean ridge from the behavior of ridge-axis discontinuities: *Nature*, v. 335, p. 217–225.
- Perfit, M.R., and Chadwick, W.W., Jr., 1998, Magmatism at mid-ocean ridges; constraints from volcanological and geochemical investigations, in Buck, W.R., et al., eds., *Faulting and magmatism at mid-ocean ridges*: American Geophysical Union Geophysical Monograph 106, p. 59–115.
- Pezard, P.A., Anderson, R.N., Ryan, W.B.F., Becker, K., Alt, J.C., and Gente, P., 1992, Accretion, structure and hydrology of intermediate-spreading-rate oceanic crust from drillhole experiments and seafloor observations: *Marine Geophysical Researches*, v. 14, p. 93–123.
- Phipps Morgan, J., and Chen, Y.J., 1993, The genesis of oceanic crust: Magma injection, hydrothermal circulation, and crustal flow: *Journal of Geophysical Research*, v. 98, p. 6283–6298.
- Rubin, A.M., 1992, Dike-induced faulting and graben subsidence in volcanic rift zones: *Journal of Geophysical Research*, v. 97, p. 1839–1858.
- Rubin, A.M., and Pollard, D.D., 1988, Dike-induced faulting in rift zones of Iceland and Afar: *Geology*, v. 16, p. 413–417.
- Shaw, W.J., and Lin, J., 1996, Models of oceanic ridge lithospheric deformation: Dependence on crustal thickness, spreading rate, and segmentation: *Journal of Geophysical Research*, v. 101, p. 17,977–17,993.
- Tucholke, B.E., and Lin, J., 1994, A geological model for the structure of ridge segments in slow spreading oceanic crust: *Journal of Geophysical Research*, v. 99, p. 11,937–11,958.
- Wilcock, W.S.D., and Delaney, J.R., 1996, Mid-ocean ridge sulfide deposits: Evidence for heat extraction from magma chambers or cracking fronts?: *Earth and Planetary Science Letters*, v. 145, p. 49–64.

Manuscript received 4 July 2005

Revised manuscript received 17 November 2005

Manuscript accepted 18 November 2005

Printed in USA

Supplementary Information

Seismic data were acquired in 2002 during *R/V Ewing* cruise EW0207 using a 6 km-long, 480 channel Syntron digital streamer with 12.5 m spaced receiver groups. Streamer depth and feathering were monitored with depth controlling and compass-enhanced DigiCourse birds, with a GPS receiver on the tail buoy. The sound source for the MCS survey was a tuned array of 10 air-guns with a total capacity of 3005 cubic inch (49.2 L), fired every 37.5 m, and towed at a nominal depth of 7.5 m. During ridge crest surveys, data were recorded at a sampling rate of 4 ms for 10.24-s-long records. Common midpoint (CMP) bin spacing is 6.25 m and the data trace fold is 81. Data are processed following a standard sequence including sorting in CMP gathers, trace editing, band-pass filtering, velocity analysis, normal moveout (NMO) correction, stacking, and migration, and a dip moveout (DMO) -based approach to suppress seafloor-scattered energy. The processing sequence was designed to enhance the stacking of two primary events; the turning energy from the base of layer 2A and the AMC reflection. Further details on the processing sequence as well as stacked and migrated sections are presented in Canales et al (in press).

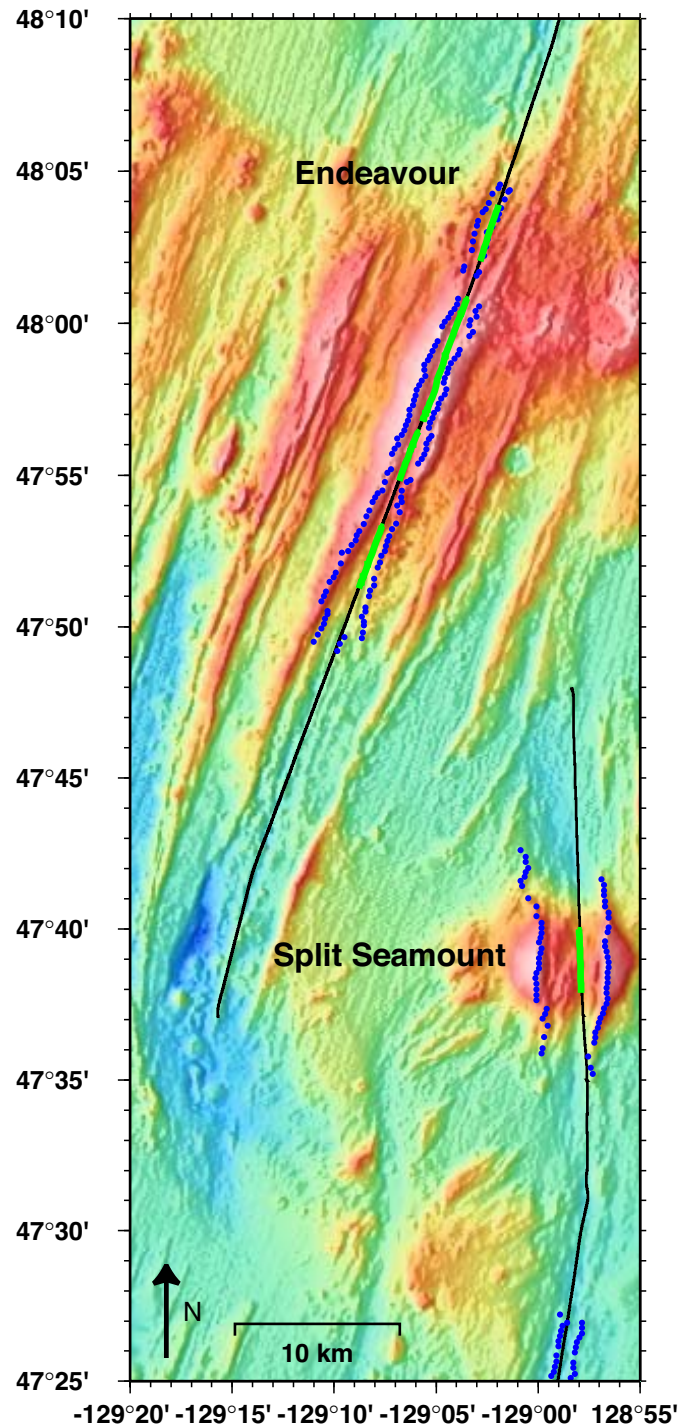


Figure DR1. Bathymetry map of Split Seamount and Endeavour segment showing spatial correlation between the axial graben and the AMC. Axial graben picks (blue dots) correspond with top of graben walls. We use an automatic method to detect the top of the graben walls based on inflection points in the bathymetry. Wide green line delineates the extent of the AMC reflection detected along seismic profiles (black lines). Note that AMC disappears north and south of Split seamount and Endeavour high as the prominent symmetric axial graben disappears. Misalignment of the survey track with the ridge axis may account for the absence of an AMC in some locations (e.g. for ~10km directly south of Split seamount), but elsewhere, the seismic profile is well centered on the axis and the AMC is absent.